Applied Mathematics & Information Sciences
An International Journal

http://dx.doi.org/10.18576/amis/180510

The Exact Endoscopic Effect and Non-Uniform Geometry on the Peristaltic Flow

F. N. M. Al-Showaikh

Department of Mathematical Sciences, Languages and General Studies, College of Arts & Science, Ahlia University, P.O. Box 10878, Manama, Kingdom of Bahrain

Received: 24 May 2024, Revised: 16 Jun. 2024, Accepted: 13 Jul. 2024
Published online: 1 Sep. 2024

Abstract: In this paper, we delve into the complex interplay of fluid mechanics, endoscopy, and non-uniform geometries within a physiological setting. We analyze the impact of an inserted endoscope on the flow of a Newtonian fluid through a non-uniform tube, employing zero Reynolds number and infinitely long wavelength approximations. Utilizing cylindrical coordinates, we formulate the problem and investigate the interplay between pressure rise, friction forces on the endoscope and outer tube, and flow rate variations. Our findings reveal that both pressure rise and friction forces acting on the endoscope and small intestine exhibit a direct correlation with increasing amplitude ratio and radius ratio, particularly at minimum and maximum flow rates. Notably, these forces become independent of both parameters at specific flow rate values. Furthermore, we explore the influence of the endoscope and amplitude ratio on peristaltic and augmented pumping mechanisms across various physical parameters. Comparisons with existing studies are drawn to enrich the understanding of this intricate phenomenon.

Keywords: Peristaltic Flow, Reynolds Number, Newtonian Fluid, Non-uniform Geometry, Endoscope

1 Introduction

It has been established that peristalsis is now well known to physiologists to be one of the major mechanisms for fluid transport in many biological systems. Accordingly, it is important to try to discuss physiological and pathological problems, when it is possible, from mathematical point of view. The authors studied peristaltic motion by assuming physiological fluids behave like Newtonian fluid are [1], [2], [3], [4], [5], [6], [7], [8], [9], [16], [10], [12], among others. Since theoretical results depend upon solutions of Navier-Stokes equations, an assumption of either inertia-free steady flow or flow with small amplitude was found convenient. These studies considered only the forced oscillation wave on a channel or a cylinder.

In this paper we are concerned with the axi-symmetric peristaltic flow of a Newtonian fluid in the gap between a non-uniform tube and uniform tube (endoscope). Our calculations are based on the definitions given by [11] regarding the pressure rise and friction force on the endoscope and non-uniform tube. The main purpose of the present study is to understand the effects of the radius ratio (the ratio between the radius of the endoscope and the radius of non-uniform tube at inlet), amplitude ratio and flow rate on pressure rise and friction forces on the endoscope and non-uniform tube.

From physiological point of view [14] observed that physiological organs are generally a non-uniform duct. Hence, peristaltic analysis of a Newtonian fluid in a uniform tube cannot be applied when explaining the mechanism of transport fluid in these organs. From mathematical point of view [16] and [12] solved the problem in steady flow (wave frame) and uniform geometry for the ureter, but we solved the problem in unsteady flow (laboratory frame) and non-uniform geometry for the small intestine.

Furthermore, the results more general than the results obtained by [14] for constant viscosity coefficient. Moreover, [16] assumed that there does not exist an overall pressure gradient over one wavelength for the normal ureter. But in our results for small intestine we have found that the pressure rise is positive, negative and zero at certain values of time parameter and flow rate. This agrees with discussion given by [12].

Also, [12] show that the important physical quantities in peristaltic pumping are sensitive to the shape of the

* Corresponding author e-mail: Falshowaikh@ahlia.edu.bh

wave in presence of the catheter which supports the hypothesis that were indicated in our paper. The theory of long wavelength and zero Reynolds number was applied as [11] and [14] in the case of there is no endoscope and physically, the presence of endoscope does not change the theory. Moreover, the present work is generalization of results obtained in [17] and [18]. If we put $s = 0$ and use the transformations given in equation (10) then we get the same results obtained by [17] and [18] for Newtonian fluids with constant viscosity. With the above discussion in mind, we proposed to study effects of endoscope and Newtonian fluid on peristaltic motion for non-uniform tube.

The paper is organized as follows. After this introduction Section 2 reviews the formulation and analysis of the model. Numerical results and discussion are discuused in Section 3. Finally, Section 4 is devoted to conclusion.

2 Formulation and Analysis

Consider the flow of an incompressible Newtonian fluid through the gap between an axi-symmetric form of a non-uniform tube and a uniform tube (an endoscope). We assume an infinite sinusoidal wave train moving with velocity c along the wall of non-uniform tube and the uniform tube is rigid.

$$\overline{r}_1 = a_1, \tag{1}$$

$$\overline{r}_2 = a(\overline{Z}) + b\sin\frac{2\pi}{\lambda}(\overline{Z} - c\overline{t}), \tag{2}$$

with

$$a(\overline{Z}) = a_2 + s\overline{Z}, \tag{3}$$

where a_1 is the radius of inner tube (the endoscope), $a(\overline{Z})$ is the radius of outer tube at any axial distance $\overline{Z}$ from inlet, a_2 is the radius of the outer tube at inlet, $s < 1$ is a constant whose magnitude depends on the length of the outer tube, exit and inlet dimensions, b is amplitude of the wave, λ is the wavelength and $\overline{t}$ is the time. We choose the cylindrical coordinates system $(\overline{R},\overline{Z})$, where $\overline{Z}-$ axis lies along the centerline of the inner and outer tubes and $\overline{R}$ is the distance measured radially. In the moving coordinates $(\overline{r},\overline{z})$ which travel in the $\overline{Z}$ direction with the same speed as the wave, the flow in the gap between the inner and outer tubes is steady but if we choose fixed coordinates $(\overline{R},\overline{Z})$, then the flow can be treated as unsteady. The coordinates frames are related through

$$\overline{z} = \overline{Z} - c\overline{t}; \overline{r} = \overline{R}, \tag{4}$$

$$\overline{w} = \overline{W} - c; \overline{u} = \overline{U}, \tag{5}$$

where $\overline{u},\overline{w}$ and $\overline{U},\overline{W}$ are the velocity components in the radial and axial directions in the moving and fixed coordinates, respectively.

Equations of motion and boundary conditions in the fixed coordinates are continuity equation

$$\frac{1}{\overline{R}}\frac{\partial(\overline{R}\,\overline{U})}{\partial\overline{R}} + \frac{\partial\overline{W}}{\partial\overline{Z}} = 0, \tag{6}$$

Navier−Stokes equations

$$\rho\left(\frac{\partial\overline{U}}{\partial\overline{t}} + \overline{U}\frac{\partial\overline{U}}{\partial\overline{R}} + \overline{W}\frac{\partial\overline{U}}{\partial\overline{Z}}\right) = -\frac{\partial\overline{P}}{\partial\overline{R}} + \mu\left(\frac{\partial^2\overline{U}}{\partial\overline{R}^2} + \frac{1}{\overline{R}}\frac{\partial\overline{U}}{\partial\overline{R}} + \frac{\partial^2\overline{U}}{\partial\overline{Z}^2} - \frac{\overline{U}}{\overline{R}^2}\right), \tag{7}$$

$$\rho\left(\frac{\partial\overline{W}}{\partial\overline{t}} + \overline{U}\frac{\partial\overline{W}}{\partial\overline{R}} + \overline{W}\frac{\partial\overline{W}}{\partial\overline{Z}}\right) = -\frac{\partial\overline{P}}{\partial\overline{Z}} + \mu\left(\frac{\partial^2\overline{W}}{\partial\overline{R}^2} + \frac{1}{\overline{R}}\frac{\partial\overline{W}}{\partial\overline{R}} + \frac{\partial^2\overline{W}}{\partial\overline{Z}^2}\right), \tag{8}$$

where ρ is the density of the fluid, μ is the coefficient of viscosity and $\overline{P}$ is the pressure. Boundary conditions:

$$\overline{W} = 0, \overline{U} = 0 \; for \overline{R} = \overline{r}_1 = a_1,$$

$$\overline{W} = 0, \overline{U} = \frac{\partial\overline{R}}{\partial\overline{t}} \; for \overline{R} = \overline{r}_2 = a_2(\overline{Z}) + b\sin\frac{2\pi}{\lambda}(\overline{Z} - c\overline{t}), \tag{9}$$

Using the dimensionless of the variables appearing in equations (1)−(9) that give Reynolds number (Re) and wave number (δ) as follows:

$$r = \frac{\overline{r}}{a_2}, R = \frac{\overline{R}}{a_2}, z = \frac{\overline{z}}{\lambda}, Z = \frac{\overline{Z}}{\lambda}, t = \frac{c\overline{t}}{\lambda}, u = \frac{\lambda\overline{u}}{a_2 c}, U = \frac{\lambda\overline{U}}{a_2 c},$$

$$w = \frac{\overline{w}}{c}, W = \frac{\overline{W}}{c}, P = \frac{a_2^2\overline{P}}{c\lambda\mu}, R_e = \frac{\rho c a_2}{\mu}, \delta = \frac{a_2}{\lambda}, \varepsilon = \frac{a_1}{a_2},$$

$$r_1 = \frac{\overline{r}_1}{a_2} = \varepsilon, r_2 = \frac{\overline{r}_2}{a_2} = 1 + \frac{\lambda s Z}{a_2} + \phi\sin 2\pi(Z - t), \tag{10}$$

where $\phi = \frac{b}{a_2}$ is the amplitude ratio and ε is the radius ratio at inlet.

Equations of motion and boundary conditions in the dimensionless form are

$$\frac{1}{R}\frac{\partial(RU)}{\partial R} + \frac{\partial W}{\partial Z} = 0, \tag{11}$$

$$Re\delta^3\left(\frac{\partial U}{\partial t} + U\frac{\partial U}{\partial R} + W\frac{\partial U}{\partial Z}\right) = -\frac{\partial P}{\partial R} + \delta^2\left[\frac{\partial}{\partial R}\left(\frac{1}{R}\frac{\partial(RU)}{\partial R}\right) + \delta^2\frac{\partial^2 U}{\partial Z^2}\right], \tag{12}$$

$$Re\delta\left(\frac{\partial W}{\partial t} + U\frac{\partial W}{\partial R} + W\frac{\partial W}{\partial Z}\right) = -\frac{\partial P}{\partial Z} + \frac{1}{R}\frac{\partial}{\partial R}\left(R\frac{\partial W}{\partial R}\right) + \delta^2\frac{\partial^2 W}{\partial Z^2}, \tag{13}$$

with the dimensionless boundary conditions

$$W = 0, U = 0 \; for R = r_1 = \varepsilon,$$

$$W=0, U=\frac{\partial R}{\partial t} \; for R=\overline{r}_2=1+\frac{\lambda s Z}{a_2}+\phi \sin 2\pi(Z-t), \tag{14}$$

Using the long wavelength approximation ($\delta=0$) then Navier−Stokes equations are reduced to:

$$\frac{\partial P}{\partial R}=0, \tag{15}$$

$$\frac{\partial P}{\partial Z}=\frac{1}{R}\frac{\partial}{\partial R}(R\frac{\partial W}{\partial R}). \tag{16}$$

Integrating equation (16), and using boundary conditions (14), we get the velocity profile as:

$$W=\frac{1}{4}\frac{\partial P}{\partial Z}[R^2-\frac{(r_1^2-r_2^2)\log R+r_2^2\log r_1-r_1^2\log r_2}{\log(r_1/r_2)}]. \tag{17}$$

The rate of volume flow in the stationary and moving coordinates are given by

$$\hat{Q}(\overline{Z},\overline{t})=\int_{\overline{r}_1}^{\overline{r}_2(\overline{Z},\overline{t})} 2\pi\overline{R}\,\overline{W}\,d\overline{R}, \tag{18}$$

$$\overline{q}(\overline{Z})=\int_{\overline{r}_1}^{\overline{r}_2(\overline{Z})} 2\pi\overline{r}\,\overline{w}\,d\overline{r}. \tag{19}$$

Substitute from equations (4) and (5) into equation (18) and make use of equation (19) then the two rates of volume flow are related through

$$\hat{Q}=\overline{q}+\pi c(\overline{r}_2^2-\overline{r}_1^2). \tag{20}$$

The time-mean flow over a period $T=\frac{\lambda}{c}$ at a fixed position $\overline{Z}$ is defined as:

$$\overline{Q}=\frac{1}{T}\int_0^T \hat{Q}(\overline{Z},\overline{t})\,d\overline{t}. \tag{21}$$

Substituting from equation (20) in equation (21) using equations (1) and (2) we obtain:

$$\overline{Q}=\hat{Q}-(2\pi a_2 cb+2\pi kcb\overline{Z})\sin\frac{2\pi}{\lambda}(\overline{Z}-c\overline{t})$$

$$-\pi cb^2\sin^2\frac{2\pi}{\lambda}(\overline{Z}-c\overline{t})+\frac{\pi cb^2}{4}. \tag{22}$$

On defining the dimensionless time-mean flow and the rate of volume flow in the stationary coordinates Θ and F as follows:

$$\Theta=\frac{\overline{Q}}{2\pi ca_2^2} \; and \; F=\frac{\hat{Q}}{2\pi ca_2^2}. \tag{23}$$

Hence, equation (22) becomes

$$F=\Theta+(1+\frac{\lambda sZ}{a_2})\phi\sin 2\pi(Z-t)+\frac{\phi^2}{2}\sin^2 2\pi(Z-t)-\frac{\phi^2}{4}, \tag{24}$$

where

$$F=\int_{r_1}^{r_2} RW\,dR. \tag{25}$$

Substituting from equation (17) in equation (25) we get

$$\frac{\partial P}{\partial Z}=\frac{16F}{r_1^4-r_2^4-((r_2^2-r_1^2)^2)/(\log r_1/r_2)}. \tag{26}$$

The pressure rise $\Delta P_\lambda(t)$ and friction forces on inner and outer tubes $F_\lambda^{(i)}(t)$ and $F_\lambda^{(o)}(t)$ are given, respectively:

$$\Delta P_\lambda(t)=\int_0^1(\frac{dP}{dZ})dZ, \tag{27}$$

$$F_\lambda^{(i)}(t)=\int_0^1 r_1^2(-\frac{dP}{dZ})dZ, \tag{28}$$

$$F_\lambda^{(o)}(t)=\int_0^1 r_2^2(-\frac{dP}{dZ})dZ. \tag{29}$$

Substituting from equations (24) and (26) in equations (27)-(29) yields

$$\Delta P_\lambda(t)=\int_0^1[\frac{16}{r_1^4-r_2^4-((r_1^2-r_2^2)^2/\log(r_1/r_2))}]\times$$

$$[\Theta+(1+\frac{\lambda sz}{a_2})\phi\sin 2\pi(Z-t)$$

$$+\frac{1}{2}\phi^2\sin^2 2\pi(Z-t)-\frac{\phi^2}{4}]dZ, \tag{30}$$

$$F_\lambda^{(i)}(t)=\int_0^1[\frac{-16r_1^2}{r_1^4-r_2^4-((r_1^2-r_2^2)^2/\log(r_1/r_2))}]\times$$

$$[\Theta+(1+\frac{\lambda sz}{a_2})\phi\sin 2\pi(Z-t)$$

$$+\frac{1}{2}\phi^2\sin^2 2\pi(Z-t)-\frac{\phi^2}{4}]dZ, \tag{31}$$

$$F_\lambda^{(o)}(t)=\int_0^1[\frac{-16r_2^2}{r_1^4-r_2^4-((r_1^2-r_2^2)^2/\log(r_1/r_2))}]\times$$

$$[\Theta+(1+\frac{\lambda sz}{a_2})\phi\sin 2\pi(Z-t)$$

$$+\frac{1}{2}\phi^2\sin^2 2\pi(Z-t)-\frac{\phi^2}{4}]dZ. \tag{32}$$

3 Numerical Results and Discussion

To discuss the results obtained above quantitatively, we shall compute the dimensionless pressure rise $\Delta P_\lambda(t)$, and friction force on inner and outer tubes for different given values of the dimensionless time mean flow Θ, amplitude ratio ϕ, and radius ratio ε. The average rise in pressure $\Delta \overline{P}_\lambda$ is then evaluated by averaging $\Delta P_\lambda(t)$ over one period of the wave. As the integrals in equations (30) to (32) are not integrable in the closed form, they are evaluated numerically using a digital computer. Following [14], we use the values of various parameters as $a_2 = 1.25\,cm$, $\lambda = 8.01\,cm$, $c = 2\,cm/min$, $s = 3a_2/\lambda$.

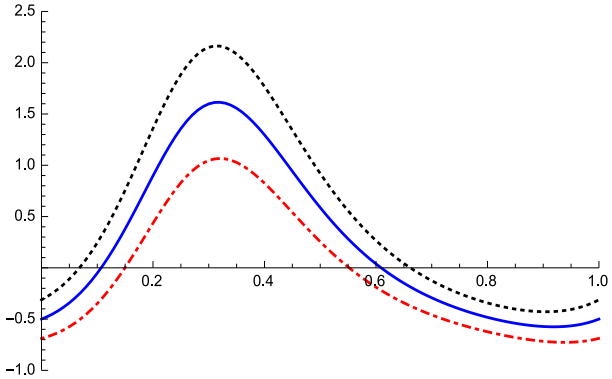

Fig. 1: The pressure rise versus time for $\phi = 0.2$ and $\varepsilon = 0.32$ for versus value of Θ, black, blue and red line for $\Theta = 0$, $\Theta = 0.05$, and $\Theta = 0.1$, respectively.

The range of mucus density is 0.95 to $3.2\,g/L$ in the small intestine as reported in [19] and the range of mucus viscosity is given as $1\,cP$ to $100\,cP$ as reported in [20]. It may be noted that the theory of long wavelength and zero Reynolds number of the present investigation remains applicable here as the radius of the small intestine, $a_2 = 1.25\,cm$, is small compared with the wavelength $\lambda = 8.01\,cm$. It has also been observed by [13] that Reynolds number in the small intestine was very small. Furthermore, since most routine upper gastrointestinal endoscopes are between 8 and $11\,mm$ in diameter as reported in [15] and the radius of the small intestine is $1.25\,cm$ as reported in [14] then the radius ratio ε takes 0.32, 0.38 and 0.44.

Equation (30) is plotted in figures (1) to (2), equation (31) is plotted in figures (3) and (4) and equation (32) is plotted in figures (5) and (6). Figures (1) and (2) show that the pressure rise increases with increasing radius ratio and it is independent of radius ratio at certain values of time parameter at $\phi = 0.2$ and $\Theta = 0.1$, but it decreases with increasing flow rate for $\phi = 0.2$ and $\varepsilon = 0.32$.

Figures (3) and (4) show the friction force on endoscope and outer tube for different values of radius ratio. It is obvious that the friction force on endoscope has

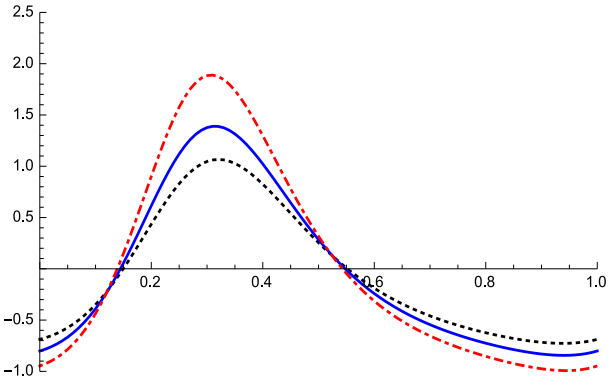

Fig. 2: The pressure rise versus time for $\phi = 0.2$ and $\Theta = 0.1$ for versus value of ε, black, blue and red line for $\varepsilon = 0.32\,\varepsilon = 0.38$, and $\varepsilon = 0.44$, respectively.

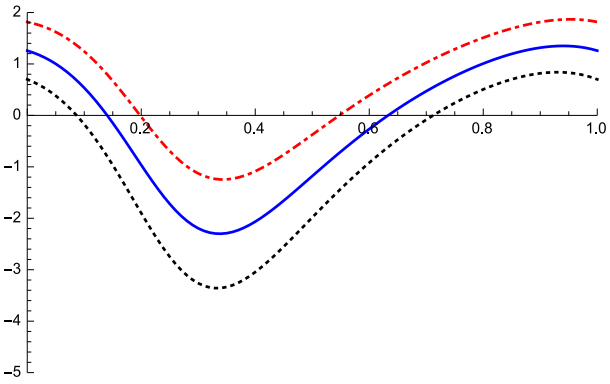

Fig. 3: The friction force on the inner tube versus time for $\phi = 0.2$ and $\Theta = 0.1$ for versus value of ε, black, blue and red line for $\varepsilon = 0.32$, $\varepsilon = 0.38$ and $\varepsilon = 0.44$, respectively.

the same direction of the wave velocity at $\{0 \le t \le 0.15, 0.55 \le t \le 1, \varepsilon = 0.32, 0.38, 0.44\}$, but it has the opposite direction of the wave velocity at $\{0.15 < t < 0.55, \varepsilon = 0.32, 0.38, 0.44\}$.

On the other hand the friction force on the outer tube has the direction of the wave velocity at $\{0 \le t \le 0.20, 0.55 \le t \le 1, \varepsilon = 0.32\}$, $\{0 \le t \le 0.21, 0.55 \le t \le 1, \varepsilon = 0.38\}$ and $\{0 \le t \le 0.22, 0.55 \le t \le 1, \varepsilon = 0.44\}$, but it has the opposite direction of the wave velocity at $\{0.20 < t < 0.55, \varepsilon = 0.32\}$, $\{0.21 < t < 0.55, \varepsilon = 0.38\}$ and $\{0.22 < t < 0.55, \varepsilon = 0.44\}$. The friction force, on the endoscope and outer tube, increases with increasing radius ratio in the same direction of the wave velocity.

However, it is independent of radius ratio at certain values of time parameter and decreases with increasing radius ratio in the opposite direction of the wave velocity.

Figures (5) and (6) show the friction force on endoscope and outer tube for different values of flow rate. It is obvious that the friction force on endoscope has the

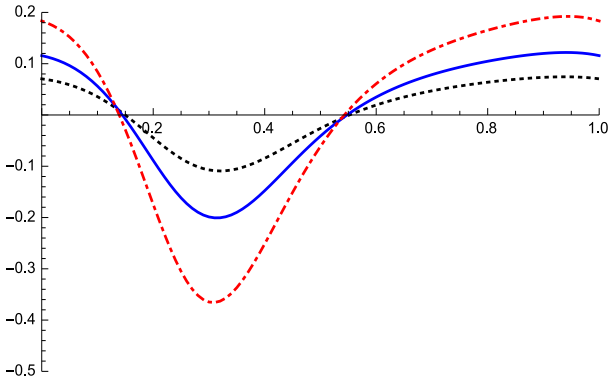

Fig. 4: The friction force on the outer tube versus time for $\phi = 0.2$ and $\Theta = 0.1$ for versus value of ε, black, blue and red line for $\varepsilon = 0.32$, $\varepsilon = 0.38$ and $\varepsilon = 0.44$, respectively.

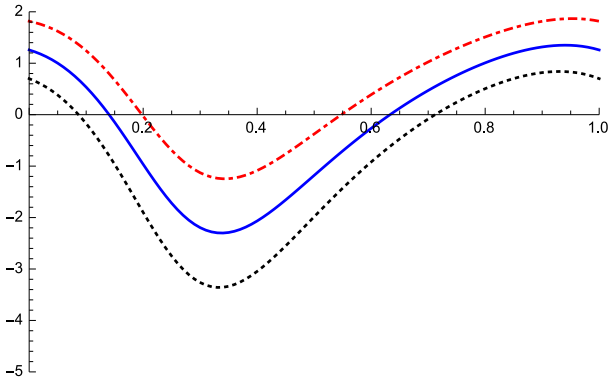

Fig. 5: The friction force on the inner tube versus time for $\phi = 0.2$ and $\varepsilon = 0.44$ for versus value of Θ, black, blue and red line for $\Theta = 0$, $\Theta = 0.05$ and $\Theta = 0.1$, respectively.

same direction of the wave velocity at $\{0 \leq t \leq 0.07, 0.67 \leq t \leq 1, \Theta = 0\}$, $\{0 \leq t \leq 0.11, 0.61 \leq t \leq 1, \Theta = 0.05\}$ and $\{0 \leq t \leq 0.15, 0.55 \leq t \leq 1, \Theta = 0.10\}$, but it has the opposite direction of the wave velocity at $\{0.07 < t < 0.67, \Theta = 0\}$, $\{0.11 < t < 0.61, \Theta = 0.05\}$ and $\{0.15 < t < 0.55, \Theta = 0.10\}$. Also, it is clear that the friction force on outer tube has the same direction of the wave velocity at $\{0 \leq t \leq 0.10, 0.73 \leq t \leq 1, \Theta = 0\}$, $\{0 \leq t \leq 0.17, 0.64 \leq t \leq 1, \Theta = 0.05\}$ and $\{0 \leq t \leq 0.22, 0.55 \leq t \leq 1, \Theta = 0.10\}$, but it has the opposite direction of the wave velocity at $\{0.10 < t < 0.73, \Theta = 0\}$, $\{0.17 < t < 0.64, \Theta = 0.05\}$ and $\{0.22 < t < 0.55, \Theta = 0.10\}$.

The friction force on the endoscope and outer tube increases with increasing flow rate in the direction of the wave velocity, but decreases with increasing flow rate in the opposite direction. Figures (3-6) illustrate that the friction force on the endoscope is lower than that on the outer tube across various flow rates and radius ratios.

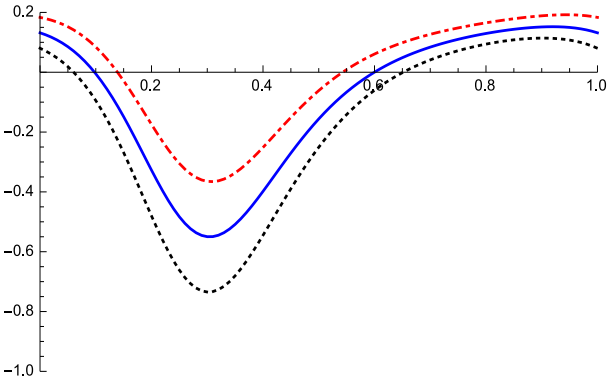

Fig. 6: The friction force on the outer tube versus time for $\phi = 0.2$ and $\varepsilon = 0.44$ for versus value of Θ, black, blue and red line for $\Theta = 0$, $\Theta = 0.05$ and $\Theta = 0.1$, respectively.

In Figure 6, we present a plot depicting the variation of the friction force on the outer tube over time. The specific parameter values chosen for this plot are $\phi = 0.2$ and $\varepsilon = 0.44$. We have represented the data using three distinct lines: a black line corresponding to $\Theta = 0$, a blue line corresponding to $\Theta = 0.05$, and a red line corresponding to $\Theta = 0.1$. Each line represents a different value of Θ, providing a comparative analysis of the friction forces for different conditions.

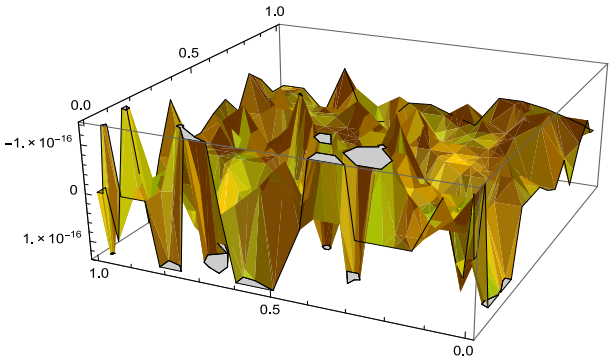

Fig. 7: Plot of the velocity versus time and Z for $\phi = 0.2$, $\varepsilon = 0.32$ and $\Theta = 0.05$.

By examining the plot, we can observe how the friction force on the outer tube changes over time for the given parameter values and Θ values. The contrasting patterns and trends exhibited by the black, blue, and red lines enable us to evaluate the influence of Θ on the friction force at various time intervals.

In comparison to the results obtained by [11], [14] for Newtonian fluid, a detailed analysis reveals significant differences in the presence of an endoscope. Specifically, the pressure rise experienced when an endoscope is

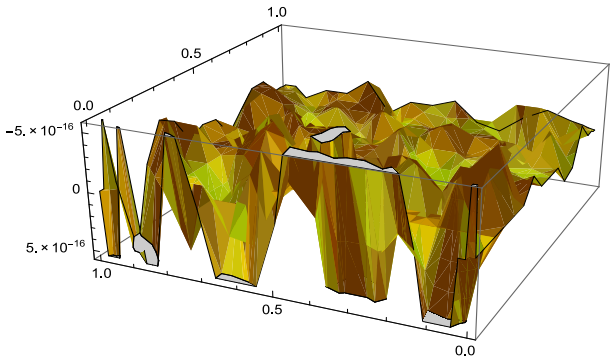

Fig. 8: Plot of the velocity versus time and Z for $\phi = 0.6$, $\varepsilon = 0.32$ and $\Theta = 0.05$.

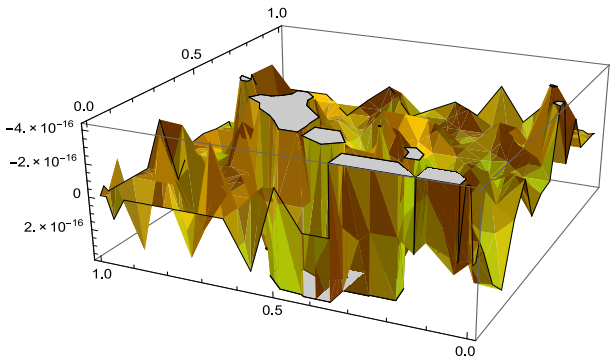

Fig. 9: Plot of the velocity versus time and Z for $\phi = 0.6$, $\varepsilon = 0.44$ and $\Theta = 0$.

present is found to be negative, indicating the absence of pumping action. This observation holds true for various values of flow rate and radius ratio at specific time parameter values. On the other hand, when the endoscope is not present, the pressure rise is positive, indicating the presence of pumping action. This is observed for different flow rates. Moreover, the effect of friction forces on both the outer tube and the endoscope is found to be positive at certain time parameter values for various flow rates and radius ratios. This positive effect leads to the existence of backward flow. Contrasting these findings, [11] and [14] demonstrated that without the endoscope, the friction force is negative for all time parameter values and different flow rates. Consequently, the absence of backward flow is observed in their study [18]−[25]. These comparative results highlight the influence of the endoscope on pressure rise, pumping action, and the presence of backward flow in the system [26]−[30].

4 Conclusion

We have investigated the intricate interplay of fluid mechanics, endoscopy, and non-uniform geometries within a physiological setting. The analysis has yielded valuable insights into the impact of an inserted endoscope on Newtonian fluid flow through a non-uniform tube. Employing simplified approximations, we elucidated the interplay between pressure rise, friction forces, and flow rate variations. Key findings reveal a direct correlation between pressure rise and friction forces on the endoscope and the surrounding tube, particularly at extreme flow rates, with a notable independence at specific intermediate values. Furthermore, the influence of the endoscope and wave amplitude on peristaltic and augmented pumping mechanisms was explored across various parameters, providing a deeper understanding of this complex phenomenon. Our findings, compared with existing studies, contribute to a more comprehensive picture of fluid-endoscope interactions within non-uniform physiological geometries.

Acknowledgement

The author is highly thankful to Ahlia University for its support.
The author is grateful to the anonymous referee for a careful checking of the details and for helpful comments that improved this paper.

References

[1] T W Latham, Fluid motion in a peristaltic pump, M S Thesis MIT Cambridge, Massachusetts (1966).
[2] A H Shapiro, M Y Jaffrin and S L Weinberg, Peristaltic pumping with long wavelength at low Reynolds number, J. Fluid Mech. **37**, 799-825 (1969).
[3] J C Burns and T Parkes, Peristaltic motion, J. Fluid Mech. **29**, 731-743 (1967).
[4] F Yin and Y C Fung, Peristaltic waves in circular cylindrical tubes, J. Appl. Mech. **36**, 579-587 (1969).
[5] P S Lykoudis and R Ross, The fluid mechanics of the ureter from lubrication theory point of view, J. Fluid Mech. **43**, 661-674 (1970).
[6] M J Manton, Long wavelength peristaltic pumping at low Reynolds number, J.Fluid Mech. **68**, 467-476 (1975).
[7] N Liron, On peristaltic flow and its efficiency, Bull.Math.Biol. **38**, 573-596 (1976).
[8] S Takabatake and K Ayukawa, Numerical study of two-dimensional peristaltic flows, J. Fluid Mech. **122**, 439-465 (1982).
[9] T F Zien and S A Ostrach, Long wave approximation to peristaltic motion, J. Biomech. **3**, 63-75 (1970).
[10] T K Mitra and S N Prasad, On the influence of wall properties and Poiseuille physiological flow in peristalsis, J. Biomech **6**, 681-693 (1973).

[11] L M Srivastava, V P Srivastava and S N Sinha, Peristaltic transport of a fluid, part I. Flow in non-uniform geometry, Biorheol. **20**, 153-166 (1983).
[12] R A Ramachandra and S Usha, Peristaltic pumping in a circular tube in the presence of an eccentric catheter, J. Biomech. Eng. **117**, 448-454 (1995).
[13] H S Lew, Y C Fung and C B Lowenstein, Peristaltic carrying and mixing of chyme in small intestine, J. Biomech. **4**, 297-315 (1971).
[14] L M Srivastava and V P Srivastava, Peristaltic transport of a non-Newtonian fluid. Applications to the vas deferens and small intestine, Annals of Biomedical Eng., **13**, 137-153 (1985).
[15] P B Cotton and X B Williams, Practical Gastrointestinal Endoscopy (Oxford, London) 3rd Edition, P.7. (1990).
[16] R Roos and PS Lykoudis, The fluid mechanics of the ureter with an inserted catheter J.Fluid Mech **46**, 625-630 (1971) .
[17] Abd El Hakeem Abd El Naby and A M El Misery, Effects of an endoscope and generalized Newtonian fluid on peristaltic motion, J. Appl. Math. Comput. **128**, (1), 19-35 (2002).
[18] A M El Misery, Abd El Hakeem Abd El Naby and Abd Hameed El Nagar, Effects of a fluid with variable viscosity and an endoscope on peristaltic motion, J. Phys. Soc. Japan **72**, (1), 89-93 (2003).
[19] G C Shit, M. Roy and A. Sinha, Mathematical modelling of blood flow through a tapered overlapping stenosed artery with variable viscosity, Appl. Bionics Biomech. **11**, 185-195 (2014).
[20] M A Nassar, Mohamed A. Ramadan and Kamal R. Raslan, Solving Natural Convection Of Darcian Fluid In Porous Media Using Rational Chebyshev Collocation Method, Appl. Math. Inf. Sci., **14**, 865-872 (2020) doi:10.18576/amis/140514.
[21] M F El-Amin, Shereen Abdel-Naeem and Nehma A. Ebrahiem, Numerical Modeling of Heat and Mass Transfer with a Single-Phase Flow in a Porous Cavity, Appl. Math. Inf. Sci., **13**, (3) 427-435 (2019) doi:10.18576/amis/130315.
[22] S R Mishra, Asmat Ara and Najeeb Alam Khan, Dissipation Effect on MHD Stagnation-Point Flow of Casson Fluid Over Stretching Sheet Through Porous Media, Inf. Sci. Lett. **7**, (1) 13-20 (2018) doi:10.18576/msl/070103.
[23] M Y Malik and Khalil-ur-Rehman, Effects of Second Order Chemical Reaction on MHD Free Convection Dissipative Fluid Flow past an Inclined Porous Surface by way of Heat Generation: A Lie Group Analysis, Inf. Sci. Lett. **5**, (2) PP: 35-45 (2016) doi:10.18576/isl/050201.
[24] K. Al-Heuseen, A.I. Aljameel and M. Kh. Alquran, The Mechanism of Charge Flow and Electric Current in Porous GaN Thin Films during Photo Electrochemical Etching, Int. J. Thin Film Sci. Tech. **11**, 89-94 (2022) doi:10.18576/ijtfst/110111.
[25] M U Awan, Muhammad Aslam Noor, Marcela V. Mihai and Khalida Inayat Noor, Generalized Coordinated Nonconvex Functions and Integral Inequalities, Appl. Math. Inf. Sci. **12**, (2) 337-344 (2018) doi:10.18576/amis/120208.
[26] M A Noor and K I Noor, Strongly log-Convex Functions, Inf. Sci. Lett. **10**, 33-38 (2021) doi:10.18576/isl/100105.
[27] M. U Awan, M A Noor and K I Noor, Hermite-Hadamard Inequalities for Exponentially Convex Functions, Appl. Math. Inf. Sci. **12**, (2) 405-409 (2018) doi:10.18576/amis/120215.
[28] M. A Noor, K I Noor and M U Awan, New Perspective of Log-Convex Functions, Appl. Math. Inf. Sci. **14**, (5) 847-854 (2020) doi:10.18576/amis/140512.
[29] M S Al-Qrinawi, El-Agez, T. M., Abdel-Latif, M. S. and Taya, S. A., Capacitance-voltage measurements of hetero-layer OLEDs treated by an electric field and thermal annealing, Int. J. of Thin Film Science and Technology, **10**, 217-226 (2021) http://dx.doi.org/10.18576/ijtfst/100311.
[30] A A Elhadary, El-Zein, A., Talaat, M., El-Aragi, G. and El-Amawy, A., Studying The Effect of The Dielectric Barrier Discharge Non- thermal Plasma on Colon Cancer Cell line, Int. J. of Thin Film Science and Technology **10**, 161-168 (2021) http://dx.doi.org/10.18576/ijtfst/100305.

F. N. M. Al-Showaikh Associate Professor in Computational Mathematics and Dean of Student Affairs at Ahlia University (AU) since January 2020. He was the Chairperson of the Department of Mathematics at University of Bahrain (UOB) from October 2017 till June 2019. He was promoted to an Associate Professor in June 2018. He was the Director of Continuous Scientific Education Program at the College of Science at UOB. He was a Director of Program Review at Quality Assurance Authority for Education and Training (QAAET) (2008 – 2010). He is a Fellow of the Higher Education Academy (HEA) in UK since 2015. He finished Postgraduate Certificate in Academic Practice (PCAP) from the University of Bahrain in 2014. He obtained the Microsoft Certified Educator (MCE) in June 2018. He is a member of many committees at the department, college, and university levels. He obtained the Kuwait Research Fellowship offered by the Kuwait Foundation for the Advancement of Sciences (KFAS), University of Cambridge, from September 2003 to February 2004. He obtained his Bachelor degree in 1989 and Master degree in 1994 from the University of Bahrain. In 1989 he was appointed as a Teaching and Research Assistant at the Department of Mathematics at UOB. He obtained his Ph.D. from Brunel University, UK, in 1998. He worked as an Assistant Professor at the Department of Mathematics from 1998 to 2017. His areas of expertise are numerical solutions of initial-value problems, boundary-value problems, parabolic partial differential equations, systems of differential equations, systems in the biomedical sciences and quantum information.